R-04-49

Colloid-facilitated radionuclide transport in single fractures: Sensitivites and scoping calculations for tracer tests at Äspö

Vladimir Cvetkovic
Royal Institute of Technology (KTH)
Division of Water Resources Engineering

August 2004

Svensk Kärnbränslehantering AB
Swedish Nuclear Fuel
and Waste Management Co
Box 5864
SE-102 40 Stockholm Sweden
Tel 08-459 84 00
+46 8 459 84 00
Fax 08-661 57 19
+46 8 661 57 19

ISSN 1402-3091
SKB Rapport R-04-49

Colloid-facilitated radionuclide transport in single fractures: Sensitivites and scoping calculations for tracer tests at Äspö

Vladimir Cvetkovic
Royal Institute of Technology (KTH)
Division of Water Resources Engineering

August 2004

Keywords: Tracer transport, Colloid-facilitated radionuclide transport, Rention in fractures, Tracer tests.

Abstract

We consider colloid-facilitated radionuclide transport (CFRT) through a single fracture between an injection point and a detection/ pumping point. The experimental conditions are assumed comparable to those of the Tracer Retention Understanding Experiments (TRUE) tests, with mean water residence time in the range 10-100 h (Winberg et al., 2000; Poteri et al., 2002). Two sorbing tracers are considered: moderately sorbing Ba and strongly sorbing Cs; tritium is also considered as a reference tracer. The two controlling parameters for the CFRT experiments are forward sorption rate α_f, and the colloidal filtration rate ϵ. A sensitivity analysis is carried out with regard to these two controlling parameters, for different experimental conditions (water residence time and injection modes), and assuming different retention conditions for the tracer in the rock matrix (limited and unlimited diffusion). We find that Cs is preferable to Ba for the CFRT tests, and that 100 h mean water residence time is preferable to 10 h. Diffusion limitations do not seem to affect the early peak of CFRT and hence need not be a concern for the experiments. Reversibility of sorption on colloids seems to have a relatively small impact on CFRT for the assumed experimental conditions. Injection conditions for the tracer do not seem to be important for CFRT tests, hence injection can be carried out in a similar manner as was done for the TRUE-1 tests (Winberg et al., 2000). Filtration of colloids can strongly reduce the impact of CFRT for $\epsilon > 0.01$ 1/h, but has a relatively modest impact for $\epsilon < 0.01$ 1/h. For $\epsilon < 0.01$ 1/h, CFRT of Cs would be detectable for α_f as low as $5{\cdot}10^{-6}$ 1/h; for increasing filtration rate, increasingly higher sorption rate is required for CFRT to be detectable. For $\epsilon > 0.01$ 1/h, we established a linear log-log relationship which is simple to use once an estimate of either α_f and/or ϵ is available; an estimate of α_f can be obtained in the laboratory using for instance a batch methodology of the type presented in Lu et al. (1998, 2000).

Chapter 1

Introduction

The TRUE program addressed radionuclide retention in crystalline rock from the laboratory scale, to the near-field scale, ca 50 m (Winberg et al., 2000; Poteri et al., 2002). The main purpose of the TRUE program was to improve the understanding of retention mechanisms and hence increase the confidence in modelling retention on the performance assessment (PA) scale. The TRUE program has revealed that retention in crystalline rocks is significant when considering dissolved radionuclides.

It is well established that small amounts of suspended particulate matter (colloids) are present in the groundwater of crystalline rocks. It is also well known that colloids may enhance transport by providing "fast lanes" for radionuclides that have been attached to them.

The study reported in Cvetkovic (2003) had the objective to evaluate the potential impact of colloid-facilitated radionuclide transport (CFRT) in crystalline rock by accounting for key processes: retention due to diffusion/sorption, site-specific variability in water residence time τ and hydrodynamic control parameter β, sorption kinetics of radionuclides on colloids (linear/bi-linear), and decay. The assumed problem configuration was analogous to the one used in Allard et al. (1991) which is a PA configuration. A sensitivity study was carried out by considering the asymptotic (steady-state) limit. It was found that for some parameter combinations, colloid-facilitated transport of Pu can be significant if advective transport is relatively rapid, with Pu discharge up to 25% of the injection rate (Cvetkovic, 2003). For rapid advective transport, filtration can reduce the total radionuclide discharge significantly, however, the *in-situ* filtration rates are currently unknown (uncertain).

To constrain parameters relevant for CFRT, and provide a data base for PA calculations, a tracer experiment is planned at Äspö to assess CFRT under field conditions. The experimental set-up would take advantage of the TRUE tests, in particular the TRUE-1 configuration. As part of the preparation for the upcoming tracer experiment on CFRT at

Äspö, we study here the basic sensitivities and provide a first set of scoping calculations for what may be expected from an in-situ CFRT experiment. The results can be useful in planning the field experiments, as well as in constraining some parameters in the laboratory.

Chapter 2

Problem formulation and objectives

We consider CFRT through a single fracture (or conducting "feature"), between an injection point (A) and detection/pumping point (B). The flow path is conceptualized as consisting of many streamlines/ trajectories (or stream-tubes). Flow velocity generally varies along a streamline, whereby the advective travel time associated with a streamline, τ, is a random variable.

Two main transport mechanisms are assumed to be at work:

- **Retention of tracer in solution.** Retention is assumed to take place essentially in the rim zone. The retention properties of the rim zone are consistent with those estimated for Feature A in TRUE-1 tests; we shall consider the case when its extent is sufficiently large such that the unlimited diffusion model is applicable, and the case when the retention zone is of finite extent (denoted as ζ [L]). Although in general all retention parameters, including ζ are spatially variable, we shall simplify the problem here and assume uniform (effective) values.

- **Colloid-facilitated transport.** We assume that the flow carries suspended particles (colloids) of given characteristics onto which the radionuclide (tracer) can attach (sorb); hence basic conditions for CFRT exist.

Our first task is to formulate a transport model for a given radionuclide from point A to point B, in solution and attached to colloids; our second task is to study the sensitivity of this transport to different system parameters and experimental conditions.

Chapter 3

Theory

Advection and dispersion through fractures coupled with retention in the rim zone are to be modelled using the dual-porosity concept (Neretnieks, 1980; Cvetkovic et al., 1999).

3.1 Simplifying assumptions

The basic assumptions/conditions for our present analysis are summarized as follows:

- Flow/advection:
  - Dominant hydrodynamic mode of transport is advection in a given fracture; longitudinal diffusion and small-scale dispersion in the fracture are neglected.
  - Groundwater flow is at steady-state.
- Retention:
  - All mass transfer reactions for radionuclides are linear.
  - Radionuclide diffusion/sorption into the immobile, water saturated rock matrix and surface sorption, are the dominant retention mechanisms.
- Colloids:
  - Colloid move with groundwater velocity.
  - Colloids can filtrate, however it is assumed that their concentration is approximately constant, either because the colloids are also generated and/or because the filtration rate is relatively small.
  - The colloid-solution tracer exchange can be described by a first-order, linear and reversible kinetic model.

3.2 Transport model

Let the total injected tracer mass be m [M] and the injection rate ϕ [1/T]. Then tracer discharge at the detection point B in the solution (denoted as J_x [M/T]) and colloid-bounded (denoted as J_y [M/T]) is given by:

$$J_x(t) = m\ \langle \phi * X \rangle \quad ; \quad J_y(t) = m\ \langle \phi * Y \rangle \tag{3.1}$$

where "*" denotes convolution, and the averaging is over all streamlines (trajectories) which constitute a flow path between the pumping and detection locations, A and B. With ϕ specified and identical for all streamlines, we have

$$J_x(t) = m\,[\phi(t)\ *\ \langle X(t) \rangle] \qquad J_y(t) = m\,[\phi(t)\ *\ \langle Y(t) \rangle] \tag{3.2}$$

If the volumetric flow rate which discharges the tracer at point B is q [L^3/T], then the measurable tracer concentration C [M/L^3] in solution at B is $J_x(t)/q$ and colloid-bounded tracer concentration is $J_y(t)/q$. In the following, we consider tracer discharge for a unit mass, i.e., for $m = 1$, referred to as normalized tracer discharge; for a pulse we then have $J_x = \langle X \rangle$ and $J_y = \langle Y \rangle$. The total normalized tracer discharge is $\langle X \rangle + \langle Y \rangle$.

Due to the random variability of hydraulic properties, the water residence time along any stream-tube (trajectory) τ is a random variable to be quantified by its probability density function (pdf), $f(\tau)$; the pdf $f(\tau)$ contains the information on advection and hydrodynamic dispersion along a flow path (e.g., Cvetkovic et al., 2000).

Taking the expected value of $\widehat{X}$ and $\widehat{Y}$ as defined in Eq. (A.7) (Appendix A), we have

$$\langle \widehat{X} \rangle = A_1 \int_0^\infty \mathrm{e}^{-\Lambda_1(s)\,\tau}\, f(\tau)\, d\tau + A_2 \int_0^\infty \mathrm{e}^{-\Lambda_2(s)\,\tau}\, f(\tau)\, d\tau$$

$$\langle \widehat{Y} \rangle = B_1 \int_0^\infty \mathrm{e}^{-\Lambda_1(s)\,\tau}\, f(\tau)\, d\tau + B_2 \int_0^\infty \mathrm{e}^{-\Lambda_2(s)\,\tau}\, f(\tau)\, d\tau \tag{3.3}$$

where $A_1, A_2, B_1, B_2, \Lambda_1$ and Λ_2 are all defined in Eq. (A.8) (Appendix A).

If the Laplace transform of $f(\tau)$ is available, then the form Eq. (3.3) enables a relatively simple computation of $\widehat{X}$ and $\widehat{Y}$ as

$$\langle \widehat{X}(s) \rangle = A_1\, \widehat{f}\,[\Lambda_1(s)] + A_2\, \widehat{f}\,[\Lambda_2(s)] \tag{3.4}$$

$$\langle \widehat{Y}(s) \rangle = B_1 \, \widehat{f}\,[\Lambda_1(s)] + B_2 \, \widehat{f}\,[\Lambda_2(s)]$$

Analytical or numerical inversion of $\widehat{f}\,[\Lambda_1(s)]$ and $\widehat{f}\,[\Lambda_2(s)]$ yields the desired solution for $\langle X \rangle$ and $\langle Y \rangle$. For finite injection with a specified injection rate, the solution is obtained by convolution. Equation (3.4) is a special case of a general solution for three-phase transport with multiple linear exchanges (Cvetkovic and Painter, 2004).

In the case of irreversible sorption with $\alpha_r \to 0$, we have

$$\langle \widehat{X} \rangle = \widehat{f}(s\,R_f + \kappa\,k\,\sqrt{s} + \alpha_f)$$

(3.5)

$$\langle \widehat{Y} \rangle = \frac{\alpha_f}{W} \left[\widehat{f}(s\,R_c + \epsilon) - \widehat{f}(s\,R_c + \epsilon + W) \right]$$

where $W(s)$ is defined in Eq. (A.10) (Appendix A).

If required, radioactive decay is accounted for in Eq. (3.4) and Eq. (3.5) by replacing s with $s + \lambda$.

Chapter 4

Assumptions for sensitivity analysis

We shall consider here the following variants in the sensitivity analysis:

1. A non-sorbing tracer (HTO), moderately sorbing tracer (Ba) and strongly sorbing tracer (Cs), consistent with the tracers used in the TRUE experiments; the interest is to see how colloids affect transport depending on the sorption properties of a tracer. The HTO does not attach to colloids and is used only for reference purposes.

2. A wide range of α_f, α_r and ϵ values are to be considered.

3. Two types of boundary conditions for transport (injection modes) will be considered: Pure pulse and pulse with a tailing, where the latter is designed to mimic injection conditions of TRUE tests; the interest is to see if/how the impact of colloids is influenced by injection conditions.

4. Two values of the mean water residence times will be considered: 10 h and 100 h, designed to cover the range of the TRUE tracer tests; the interest is to see if and how water residence time affects CFRT. The effective aperture for the mobile zone (fracture) is assumed as $2b = 1$ mm.

5. A finite and an infinite retention zone will be considered, i.e., limited and unlimited diffusion will be considered for retention; the purpose is to see how CFRT is affected by diffusion limitations. The effective porosity of the retention zone is assumed as $\theta = 0.02$, with a density of $\rho = 2700$ kg/m^3. The formation factor F is computed using Archie's law as $F = \theta^{1.5} = 0.0028$. The effective thickness of the retention zone (for the limited diffusion case) is assumed as $\zeta = 2$ mm.

We discuss the assumptions related to each parameter separately.

4.1 Sorption on colloids

Colloidal concentration C_c is available from borehole measurements at various locations at the Äsp¨o site; C_c was found to depend strongly on salinity. From Figure 5 in Laaksoharju (2002, "Status report of the colloid experiment at Äspö HRL tunnel in Sweden", unpublished), we selected $C_c = 0.025$ mg/L from borehole KA3110A for moderate salinity of 3000 mg Cl^-/L as representative for the Äspö site (Cvetkovic, 2003). For this value of $_c$, an estimate of $\alpha_f = 0.001 - 0.1$ 1/yr (or $\alpha_f = 10^{-7} - 10^{-5}$ 1/h) was made and considered in sensitivity analysis of Cvetkovic (2003). Here we shall assume that in the CFRT tests, the colloidal concentration would be higher than the background concentration under natural conditions of $C_c = 0.025$ mg/L, by at least a factor 100 (say around 1 mg/L). For sensitivity analysis, we shall assume a higher range of 0.0001-0.1 1/h for α_f, but also investigate the low range case of $\alpha_f = 10^{-6}$ 1/h.

We define a reversibility ratio f_r as $\alpha_r/\alpha_f = f_r$; we shall consider the range $f_r = 0 - 0.1$, where $f_r = 0$ represents irreversible sorption, and 0.1 implies relatively strong reversibility.

4.2 Injection conditions

We assume a general form of the injection as a pulse followed by an exponentially decaying tail:

$$\phi(t) = (1-\mu)\,\delta(t) + \frac{\mu}{d_0}\,\mathrm{e}^{-t/d_0} \qquad ; \qquad \widehat{\phi}(s) = (1-\mu) + \frac{\mu}{d_0}\,\frac{1}{s+1/d_0} \tag{4.1}$$

The two controlling parameters are the fraction μ which quantifies how much of the injected tracer mass is in the pulse and how much in the tail, and decay time d_0 [T] which quantifies the duration (or extent) of the tailing in the injection. For $\mu = 0$ we have a pure (ideal) pulse, whereas for $\mu = 1$, all injected mass is in the tail. For increasing d_0, a thinner and thinner tail extends over longer and longer times; for $d_0 \to 0$ we also recover a pulse.

In our following calculations, we shall assume $d_0 = 0.05$ years (440 h). Since $\ln 2\, d_0 = 0.035$ years (300 h) is the half-life of the injection tail (i.e., the time when half of the tracer mass contained in the tail has been released), we see that for $d_0 = 0.05$ yr, the injection effectively terminates after ~ 1000 h. This is in the range that was applicable for TRUE-1 experiments, at least for more sorbing tracers. Note that in the TRUE-1 tests, for instance, the injection tailing is initially not exponential, as a peak is visible after the pulse part of the injection terminates (Winberg et al., 2000; Cvetkovic et al., 2000). Although this peak

is not captured by our current model, the measured asymptotic form of the injection tailing is reasonably approximated by exponential decay, Eq.(4.1).

4.3 Advective travel times

To apply Eq.(3.4) or Eq. (3.5), we require $f(\tau)$. For illustration purposes, we shall assume a Fickian (advection-dispersion) form of $f(\tau)$ as[1]

$$f(\tau) = \frac{c\,\mathrm{e}^{c\sqrt{a}}}{2\sqrt{\pi\tau^3}}\,\exp\left(-a\,\tau - \frac{c^2}{4\,\tau}\right) \tag{4.2}$$

where

$$a \equiv \frac{\tau_m}{2\sigma_\tau^2} \quad ; \quad c \equiv \frac{\tau_m^{3/2}\sqrt{2}}{\sigma_\tau} \tag{4.3}$$

τ_m is the mean water residence time for a given flow path (i.e., averaged over all trajectories of a flow path), and σ_τ^2 is the variance.

The Laplace transform of $f(\tau)$ Eq.(4.2) is

$$\widehat{f}(s) = \exp\left(c\,\sqrt{a} - c\sqrt{a+s}\right) \tag{4.4}$$

We shall assume in this analysis the coefficient of variation $CV(\tau) \equiv \sigma_\tau/\langle\tau\rangle = 0.5$ to be given (fixed), a value corresponding approximately to the TRUE-1 tests. Two values of the mean water residence time τ_m are to be considered in the computations, 10 h and 100 h; the former corresponds to a shorter flow path and/or higher pumping rate, whereas the latter corresponds to a longer flow path and/or lower pumping rate.

4.4 Tracer selection

We shall consider three tracers: tritium (HTO), barium (Ba) and cesium (Cs). The retention parameters D_w and K_d are tracer-dependent and are specified in Table 4.1. The values D_w are given in Byegård et al. (1998), while K_d are close to calibrated values for TRUE-1 (Cvetkovic et al., 2000). The pore diffusivity in $\kappa = \theta\sqrt{R_m\,D}$ is related to D_w as $D = D_w\,F/\theta$ where F is the formation factor. The retardation coefficient for the matrix is computed as $R_m = 1 + \rho K_d/\theta$.

[1] In a subsequent chapter, we show how the parameters a and c can be related to the classical advection-dispersion parameters, the mean velocity and longitudinal dispersion coeffi cient.

Table 4.1: Summary of data for HTO, Ba and Cs used in the calculations.

TRACER	D_w $\times 10^{-6}$ [m^2/h]	K_d [m^3/kg]
Tritium	8.4	–
Barium	3	0.001
Cesium	7.3	0.05

Chapter 5

Results

In this chapter we present results of the sensitivity analysis and scoping calculations. When referring to expected tracer discharge $\langle X \rangle$ and $\langle Y \rangle$, we shall for simplicity omit the angular brackets and in the following refer to X and Y. Also, we shall neglect the effects of surface sorption and retardation of colloids, setting $R_f = R_c = 1$. Because the experimental transport times are relatively short, we also neglect radioactive decay, i.e., $\lambda = 0$.

5.1 Pulse with unlimited diffusion

In Fig. 5.1- 5.4 we show the breakthrough curves for Ba and Cs assuming water residence time in the range $\tau_m = 10 - 100$ h, and considering pulse injection. Irreversible sorption on colloids is assumed ($f_r = 0$). The forward sorption rate α_f is considered in the range 0.0001-0.1 1/h. For comparative purposes, we plot in Fig. 5.1 five curves. As a reference, the BTC of HTO is also plotted; in the limit, for a sufficiently large forward sorption rate, the BTC of Ba or Cs would resemble the BTC of HTO. We plot tracer discharge in solution (X), tracer discharge bounded on colloids (Y), and the total normalized discharge , i.e., $X + Y$. Finally, we plot the BTC in the case when colloids are not present; this roughly corresponds to the measured BTC in either the TRUE-1 tests (for τ_m=10 h), or in the TRUE Block Scale tests (for τ_m=100 h).

5.1.1 Barium

Discharge of Ba for $\tau_m = 10$ h is shown in Fig. 5.1. Because of relatively weak retention properties of Ba, the time of the peak arrival without colloids is not very different from that of HTO, with a peak lower by a factor say 3-4 (Fig. 5.1). The peak of the colloid-bounded Ba discharge Y is approximately three orders of magnitude lower than the peak of Ba discharge in solution X (hence in this case $X + Y$ is essentially equivalent to X),

for a low sorption rate of $\alpha_f = 0.0001$ 1/h (Fig. 5.1). With an increasing forward sorption rate, the colloid-bounded peak Y increases such that it is around one order of magnitude lower than the peak of Ba discharge in solution X (Fig. 5.1 with $\alpha_f = 0.1$ 1/h). The total Ba discharge $X+Y$, discharge without colloids and discharge in solution with colloids X, all coincide for α_f in the range 0.0001-0.01 1/h (Fig. 5.1). Only for $\alpha_f = 0.1$ 1/h, do the BTCs start to differentiate, however, from the experimental point of view, these differences are small (Fig. 5.1 with $\alpha_f = 0.1$ 1/h).

The discharge of Ba for a longer mean water residence time of $\tau_m = 100$ h is shown in Fig. 5.2; longer water residence time can be either due to a longer flow path and/or due to a lower pumping rate. For $\tau_m = 100$ h, the impact of colloids is more apparent. Whereas the Ba discharge in solution X is practically indistinguishable from the total discharge $X+Y$, and also indistinguishable from the Ba discharge without colloids, the colloid bounded discharge Y has a peak that is less than two orders of magnitude lower, even for a relatively low α_f (Fig. 5.2 with $\alpha_f = 0.0001$ 1/h). As the forward sorption rate α_f increases and the tracer is transfered onto colloids at an increasing rate, the colloid-bounded peak of Y increases, whereas the peak discharge in solution X decreases. For $\alpha_f = 0.1$ 1/h, for instance, the total Ba discharge $X+Y$, and the colloid-bounded discharge Y, both coincide with the HTO discharge with a peak that is three orders of magnitude larger than for Ba discharge in solution X (Fig. 5.2 with $\alpha_f = 0.1$ 1/h).

5.1.2 Cesium

Discharge of Cs for $\tau_m = 10$ h is shown in Fig. 5.3. The retention properties of Cs are relatively strong; hence the time of the peak arrival without colloids differs about two orders of magnitude from that of HTO.[1] The peak of the colloid-bounded Cs discharge Y is approximately two orders of magnitude lower than the Cs peak discharge in solution X (hence in this case $X+Y$ is essentially equivalent to X), for a sorption rate of $\alpha_f = 0.0001$ 1/h (Fig. 5.3). The colloid-bounded peak Y increases with an increasing forward sorption rate α_f, and overtakes the peak of Cs discharge in solution X for α_f in the range 0.001-0.01 1/h; for $\alpha_f = 0.1$ 1/h, the peak of the total Cs discharge $X+Y$ is about two orders of magnitude higher than the Cs peak discharge without colloids even for a relatively short mean water residence time (Fig. 5.3).

With increasing τ_m, the impact of colloids is more apparent (Fig. 5.4). Even for the

[1] Note that we have not included here surface sorption, hence this difference is somewhat larger for the experimental BTCs of TRUE-1 and TRUE Block Scale.

lowest α_f considered of 0.0001 1/h, an early peak appears at ca 100 h due to presence of colloids and is in magnitude half of the peak of Cs discharge in solution which arrives much later (ca 30 000 h) (Fig. 5.4 with $\alpha_f = 0.0001$ 1/h). As α_f increases, the magnitude of the early peak increases, such that for $\alpha_f = 0.1$ 1/h it is 400 times larger than the Cs peak without colloids (Fig. 5.4 with $\alpha_f = 0.1$ 1/h); in this case, the Cs BTC is comparable to the BTC of HTO.

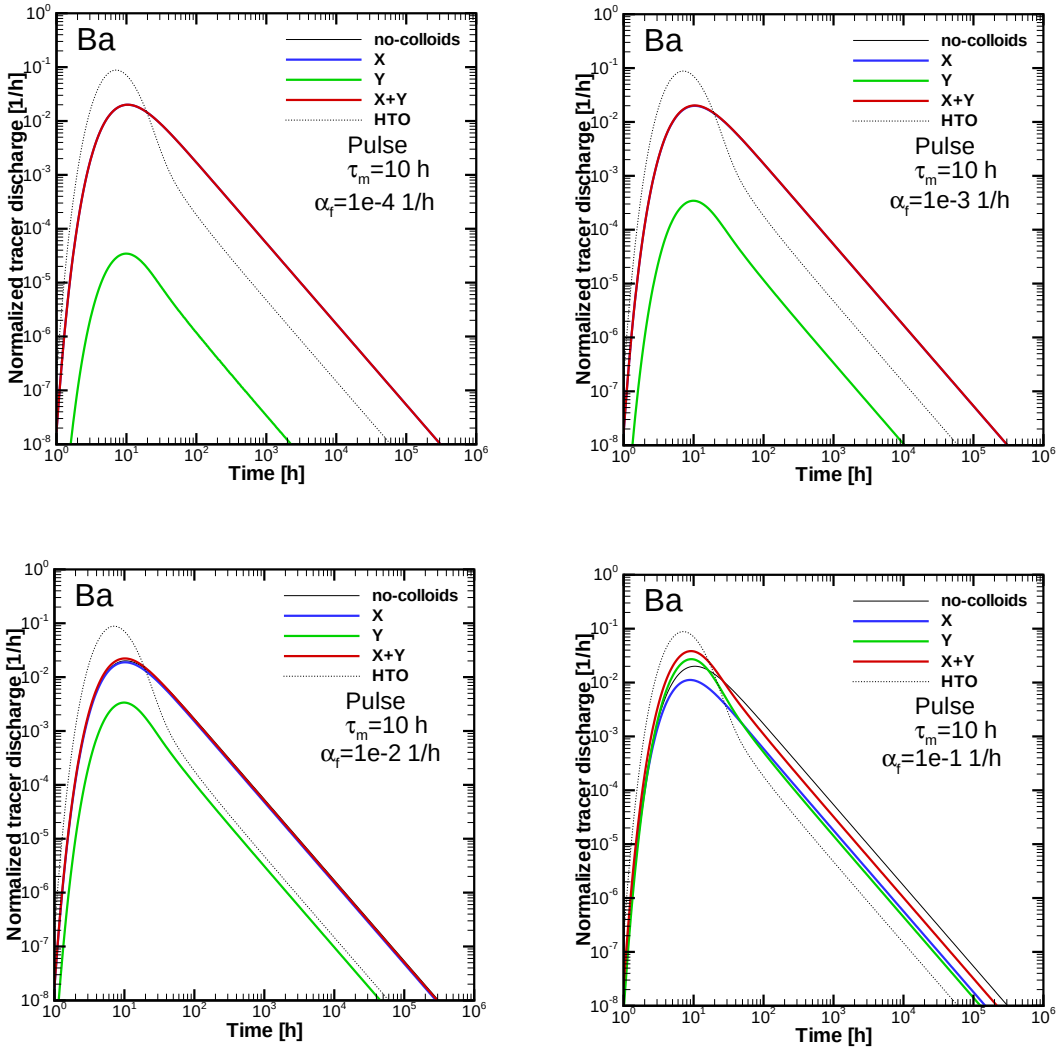

Figure 5.1: Normalized expected Ba discharge for a pulse of unit mass, and mean water residence time of 10 h. For simplicity, we omit angular brackets on X and Y. Expected discharge of HTO is included as a reference. The curves for X and Y are obtained by numerical Laplace inversion of Eqs. (3.5) with Eq. (4.4). Colloid filtration is neglected, i.e., $\epsilon = 0$.

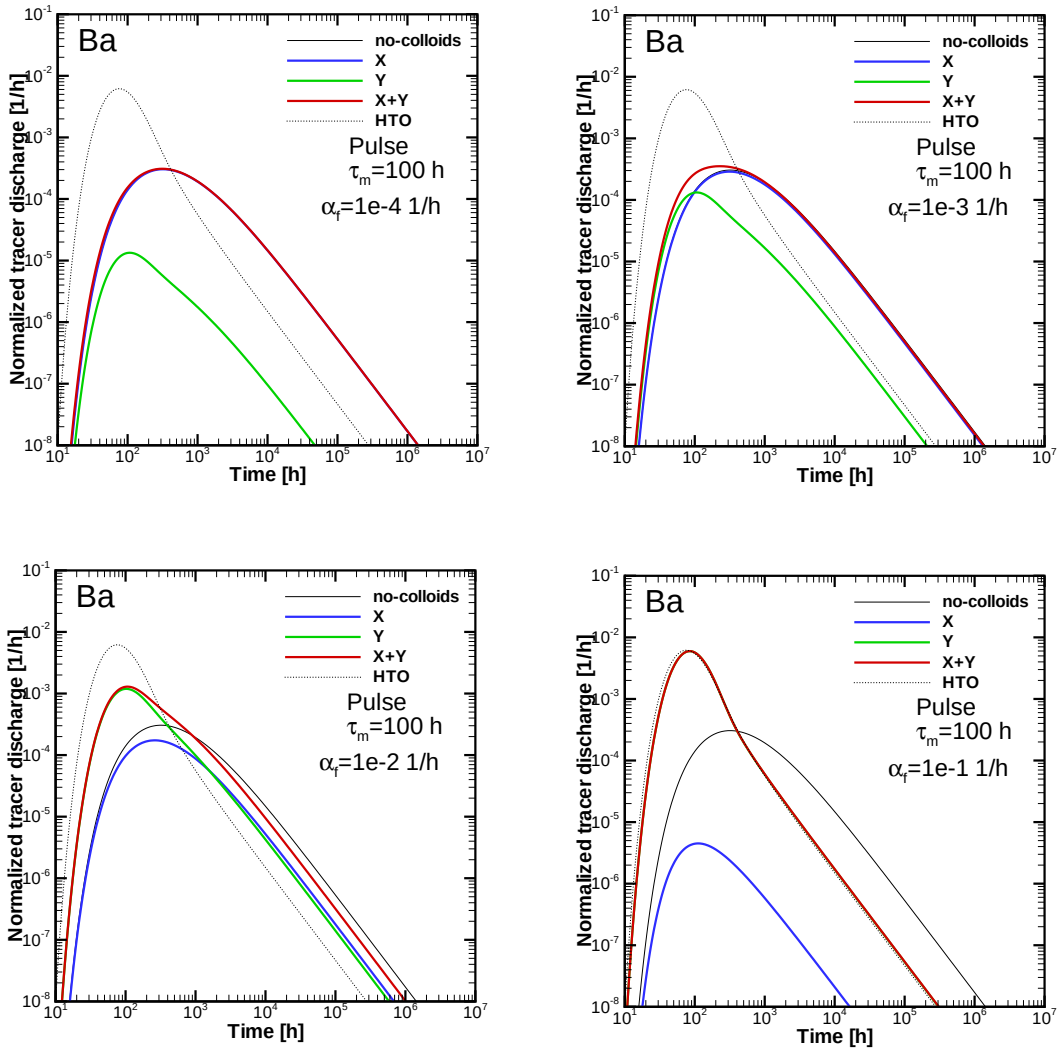

Figure 5.2: Normalized expected Ba discharge for a pulse of unit mass, and mean water residence time of 100 h. For simplicity, we omit angular brackets on X and Y. Expected discharge of HTO is included as a reference. The curves for X and Y are obtained by numerical Laplace inversion of Eqs. (3.5) with Eq. (4.4). Colloid filtration is neglected, i.e., $\epsilon = 0$.

5.2 Effect of finite injection

In Fig. 5.5 we illustrate the BTC of Cs for the longer water residence time of $\tau_m = 100$ h, i.e., under conditions identical to those of Fig. 5.4 but with finite injection. The assumed value of "pulse-tail" distribution mass fraction μ is 0.8 and the tail duration is $d_0 = 0.05$ yr, consistent with what is applicable for TRUE-1 tests. We find that finite injection does not change the Cs discharge with and without colloids significantly; the main difference is that the peak magnitude is somewhat lower (compare BTCs of Fig. 5.4 with those of Fig. 5.5).

5.3 Effect of diffusion limitations

We consider here transport conditions identical to those of Fig. 5.4 except that the retention (rim) zone is of finite extent; we assume ζ =2 mm. Clearly, the diffusion limitations affect the later part of the breakthrough, resulting in a steep drop in the tail. However, the initial part of the Cs BTCs, even for a relatively limited retention zone of 2 mm, is not affected by diffusion limitations. From an experimental point of view, the initial part of the BTC, and in particular the peaks, are important for establishing the impact of colloids. We see that the early peak due to the presence of colloids is maintained even for a finite retention zone, but with a somewhat reduced magnitude (Fig. 5.6).

5.4 Effect of sorption reversibility

The effect of sorption reversibility is quantified by the ratio $f_r = \alpha_r/\alpha_f$. In Fig. 5.7, we show the impact of reversibility for $f_r = 0.1$ on the BTCs of Cs. For the two lower values of α_f, 0.0001 and 0.001 1/h, reversibility has no impact. For $\alpha_f = 0.01$ 1/h, sorption reversibility reduces slightly the peak of $X + Y$, and increases the peak of Cs in solution as quantified by X. In other words, the effect of reversibility is to increase the discharge of Cs in solution and decrease the discharge of Cs that is colloid-bounded, Y. The effect of sorption reversibility is most apparent for largest value of $\alpha_f = 0.1$ 1/h, when the peak of $X + Y$ is reduced by a half, and the Cs discharge in solution X increases for early times (compare Fig. 5.4 and Fig. 5.7). However, the overall impact of reversibility is relatively small even in this case.

5.5 Effect of filtration

It is well known that filtration can affect CFRT significantly. In fact, filtration is viewed as the potential mechanism which can entirely eliminate CFRT. The problem however is that the field-scale filtration rates have yet to be realistically estimated. The filtration rate ϵ is therefore also treated as a sensitivity parameter.

We consider conditions for CFRT for Cs identical to those of Fig. 5.4 except that we introduce filtration; the resulting total discharge curves $X + Y$ are presented in Fig. 5.8 for the range ϵ =0.001-0.5 1/h. Comparing Fig. 5.4 (for $\alpha_f = 0.0001$ 1/h) with Fig. 5.8, we see that up to $\epsilon = 0.01$ 1/h, the impact of filtration is relatively small. For $\epsilon > 0.01$ 1/h, filtration reduces the impact of CFRT rapidly, effectively eliminating it for $\epsilon > 0.1$ 1/h.

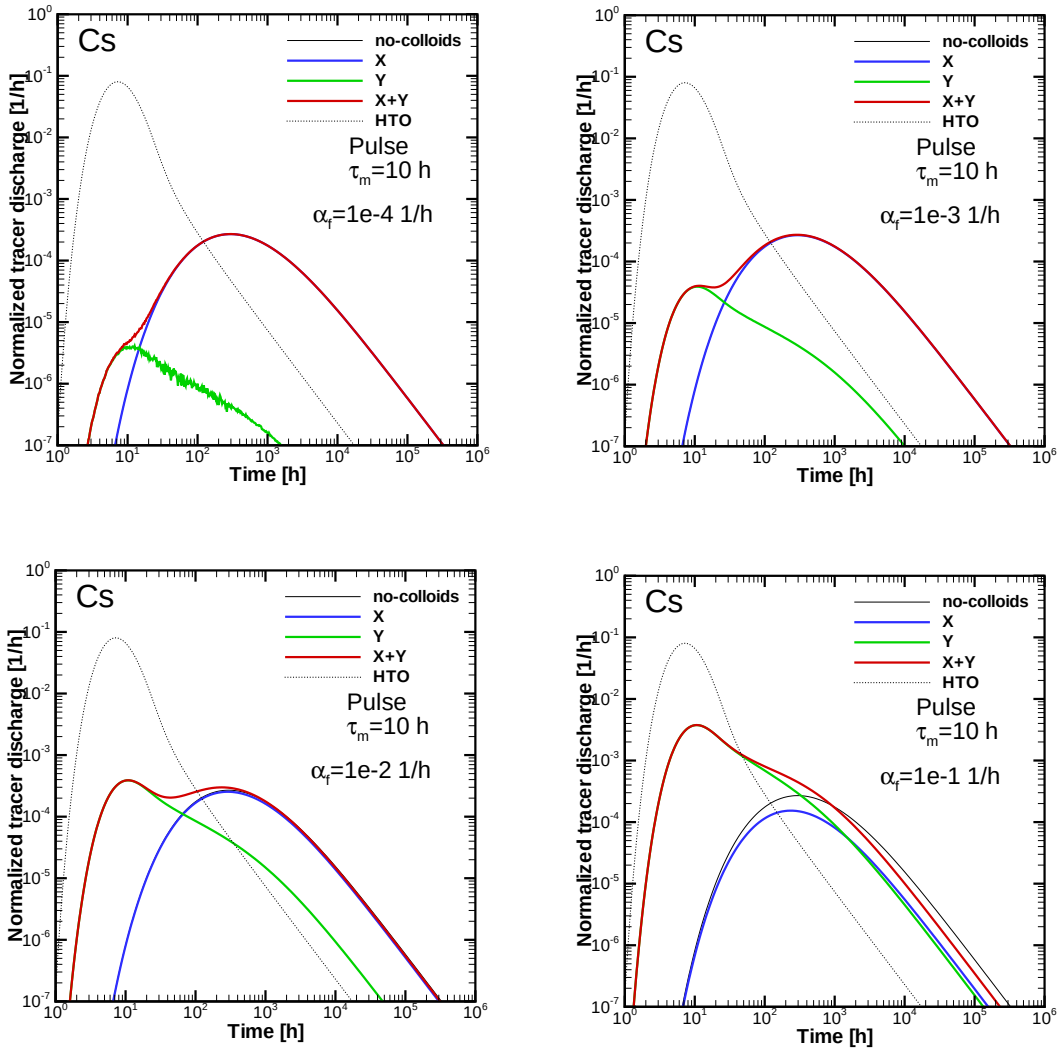

Figure 5.3: Normalized expected Cs discharge for a pulse of unit mass, and mean water residence time of 10 h. For simplicity, we omit angular brackets on X and Y. Expected discharge of HTO is included as a reference. The curves for X and Y are obtained by numerical Laplace inversion of Eqs. (3.5) with Eq. (4.4). Colloid filtration is neglected, i.e., $\epsilon = 0$.

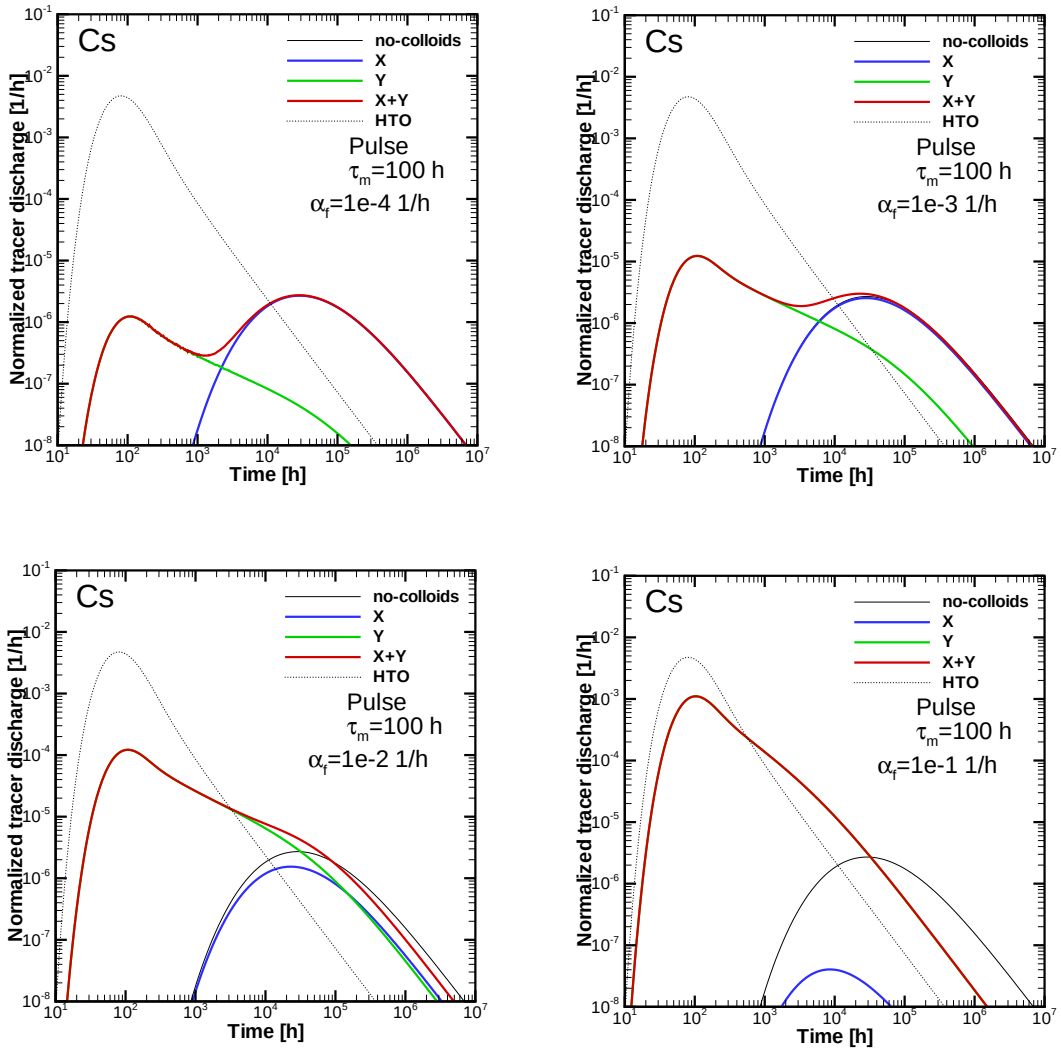

Figure 5.4: Normalized expected Cs discharge for a pulse of unit mass, and mean water residence time of 100 h. For simplicity, we omit angular brackets on X and Y. Expected discharge of HTO is included as a reference. The curves for X and Y are obtained by numerical Laplace inversion of Eqs. (3.5) with Eq. (4.4). Colloid filtration is neglected, i.e., $\epsilon = 0$.

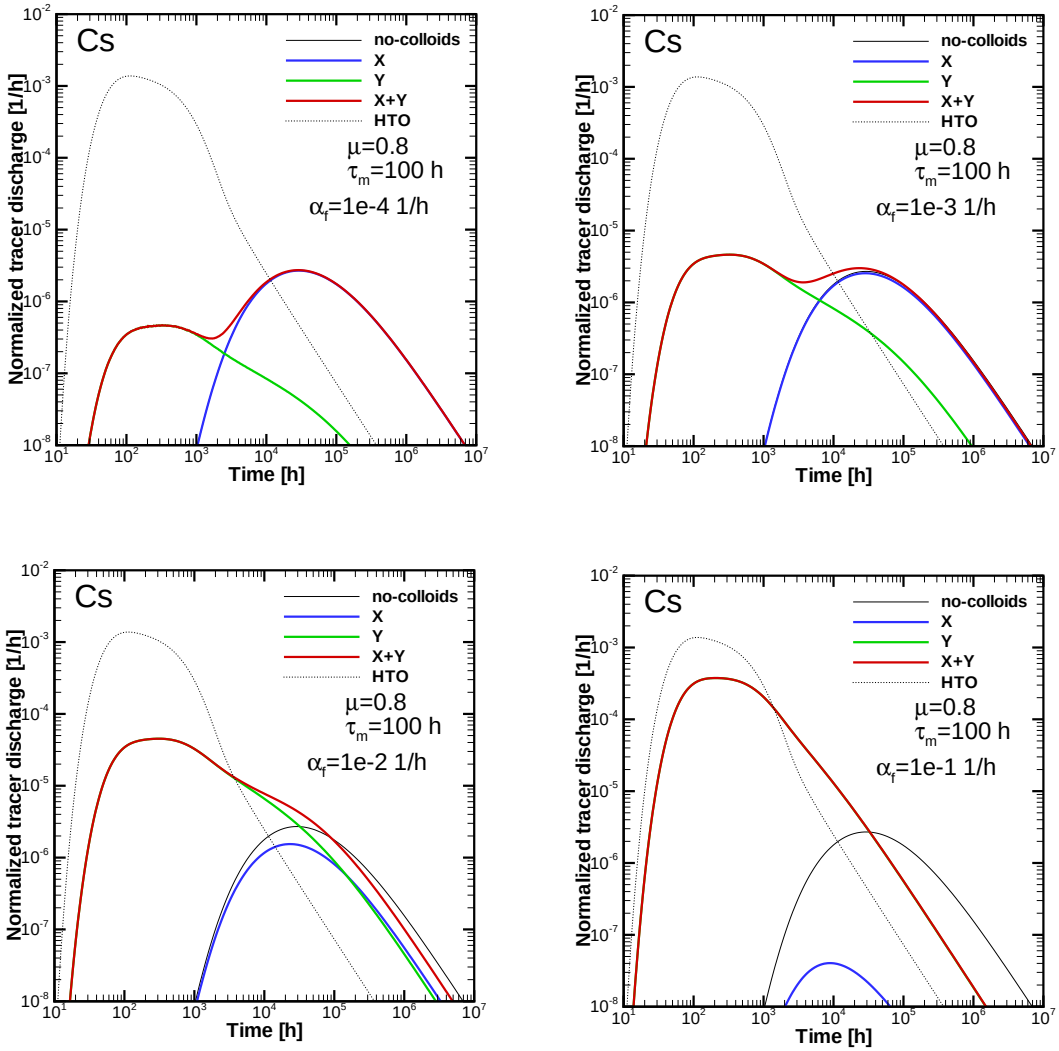

Figure 5.5: Normalized expected Cs discharge for a pulse of unit mass, and mean water residence time of 100 h. The injection is finite following Eq. (4.1). For simplicity, we omit angular brackets on X and Y. Expected discharge of HTO is included as a reference. The curves for X and Y are obtained by numerical Laplace inversion of Eqs. (3.5) with Eq. (4.4). Colloid filtration is neglected, i.e., $\epsilon = 0$.

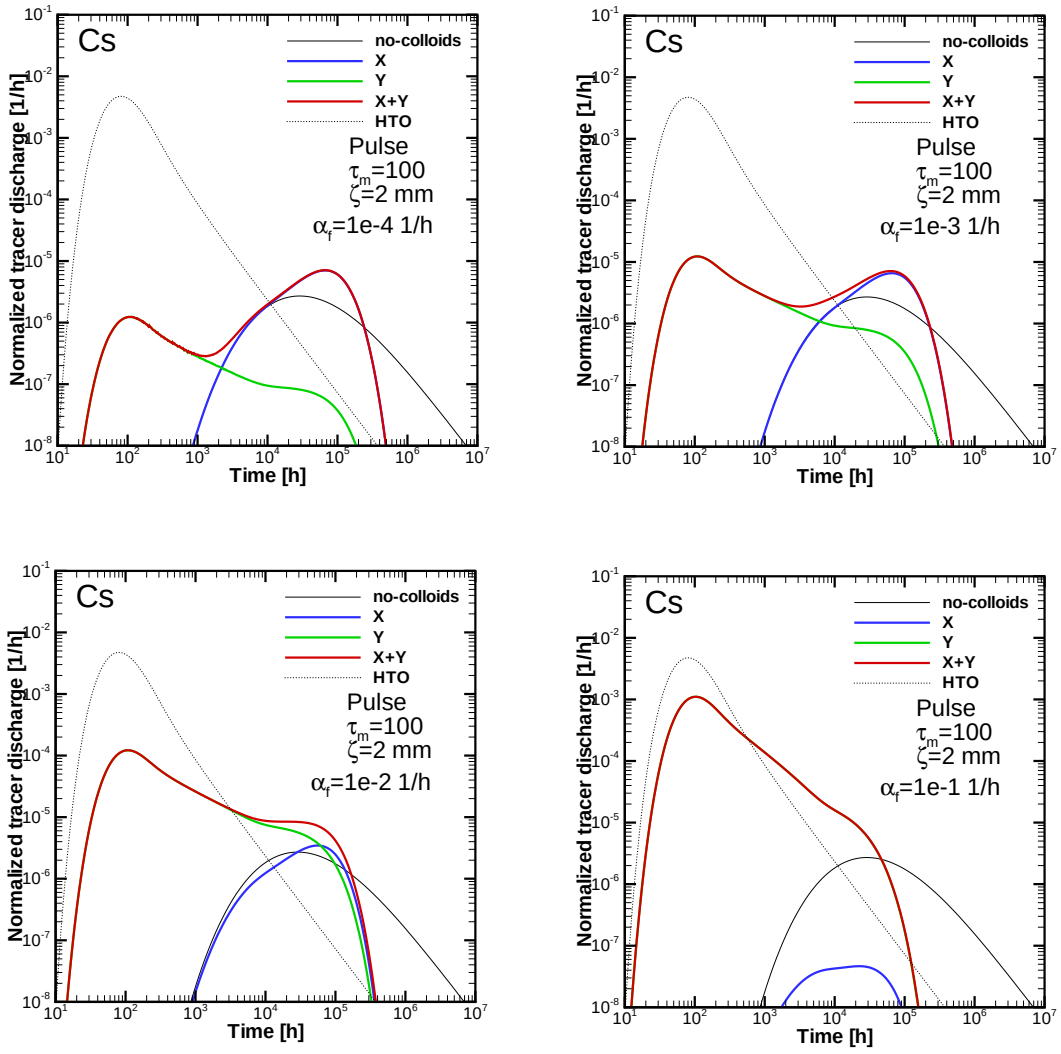

Figure 5.6: Normalized expected Cs discharge for a pulse of unit mass, and mean water residence time of 100 h. The retention zone is assumed of finite extent of an effective thickness $\zeta = 2$ mm. For simplicity, we omitted angular brackets on X and Y. Expected discharge of HTO is included as a reference. The curves for X and Y are obtained by numerical Laplace inversion of Eqs. (3.5) with Eq. (4.4). Colloid filtration is neglected, i.e., $\epsilon = 0$.

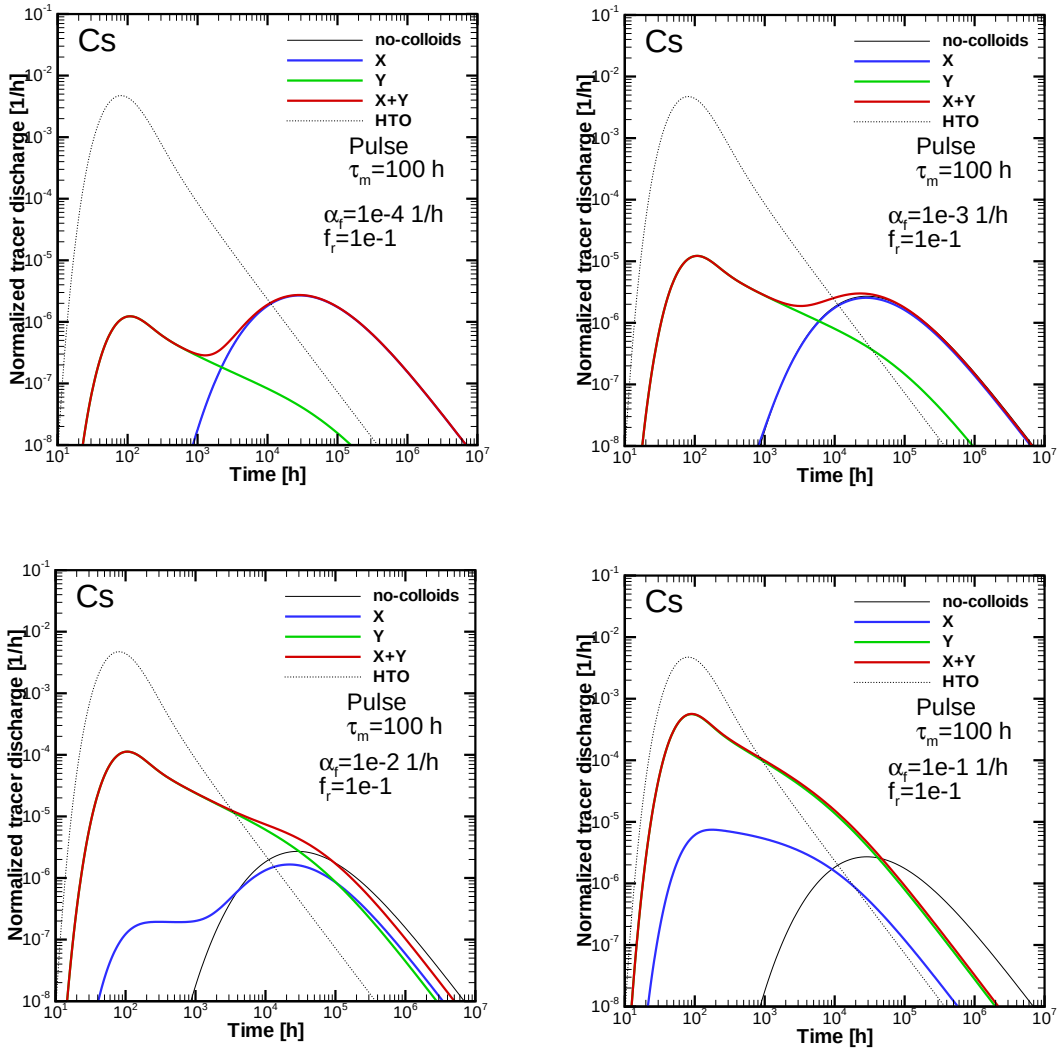

Figure 5.7: Normalized expected Cs discharge for a pulse of unit mass, and mean water residence time of 100 h. Sorption on colloids is assumed to be reversible. For simplicity, we omit angular brackets on X and Y. Expected discharge of HTO is included as a reference. The curves for X and Y are obtained by numerical Laplace inversion of Eqs. (3.4) with Eq. (4.4). Colloid filtration is neglected, i.e., $\epsilon = 0$.

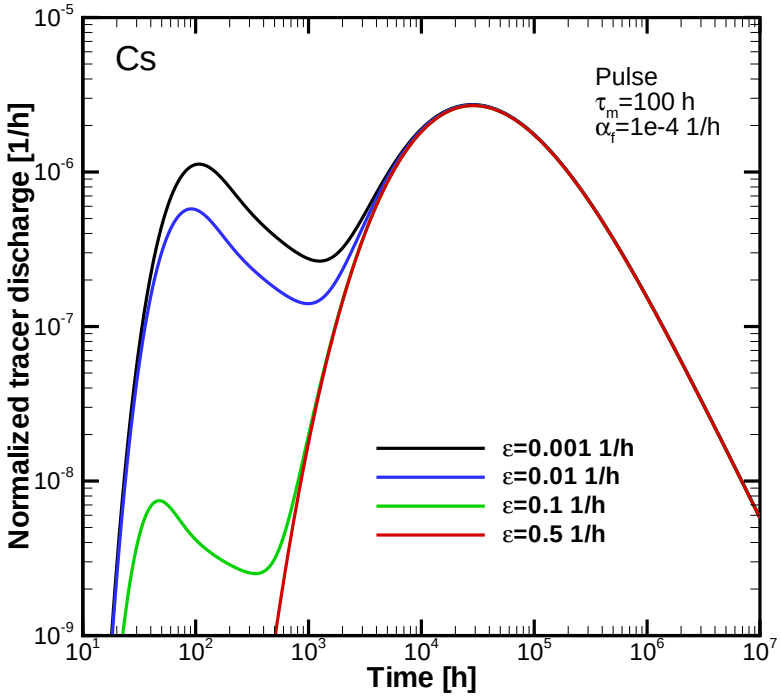

Figure 5.8: Normalized expected Cs discharge for a pulse of unit mass, and mean water residence time of 100 h. For simplicity, we omit angular brackets on X and Y. The curves for X and Y are obtained by numerical Laplace inversion of Eqs. (3.5) with Eq. (4.4). The effect of colloid filtration is illustrated for ϵ in the range 0.001-0.5 1/h.

Chapter 6

Discussion

6.1 Theoretical considerations

We shall to provide here a link between our Lagrangian approach and the more classical continuum approaches for tracer transport in crystalline rock with matrix diffusion and sorption, here in the presence of colloids.

The mass balance equations in a one-dimensional formulation (often used in field-scale applications) are written as

$$R_f \frac{\partial C}{\partial t} + U \frac{\partial C}{\partial x} - D_L \frac{\partial^2 C}{\partial x^2} = -\left(\frac{S_f D \theta}{n_f}\right) \frac{\partial C^*}{\partial z} \mid_{z=0} -\alpha_f C + \alpha_r S - \lambda R_f C \quad (6.1a)$$

$$R_c \frac{\partial S}{\partial t} + U \frac{\partial S}{\partial x} - D_L \frac{\partial^2 S}{\partial x^2} = \alpha_f C - \alpha_r S - \epsilon S - \lambda R_c S \quad (6.1b)$$

$$R_m \frac{\partial C_m}{\partial t} = D \frac{\partial^2 C_m}{\partial z^2} - \lambda R_m C_m \quad (6.1c)$$

where C [M/L] is an averaged tracer concentration in the fractures for an appropriately defined rock volume (REV), C_m [M/L] tracer concentration in the rock matrix of the rock for the REV, U [L/T] is the mean flow velocity, n_f [-] is the flow porosity, S_f [1/L] is the fracture density (defined as fracture area per bulk volume of the REV), D_x [L^2/T] is the coefficient of longitudinal dispersion, x [L] is the longitudinal spatial coordinate in the direction of the mean flow, and z [L] is the spatial coordinate orthogonal to the surface of an "effective" (representative) fracture for the REV. In other words, the system of interconnected fractures of the REV are substituted by a single representative, or effective fracture with an effective aperture $2b = 2n_f/S_f$. The other parameters are defined in Appendix A. If colloids are not present, then $\alpha_f = \alpha_r = 0$ and the above system reduces to the classical continuum form of the transport equations with Fickian diffusion and sorption in the rock matrix (e.g., Shapiro, 2001).

In the presence of colloids, Eqs. (6.1a)- (6.1c) are equivalent to the equations used in

the computations of Klos et al. (2002), if the effect of immobilized colloids on sorption is neglected (i.e., $\kappa_2 = 0$ in the Eqs.(1)-(2) of Klos et al. (2002)). Also, filtration (i.e., irreversible colloidal removal) is explicitly accounted for in Eqs. (6.1a)- (6.1c) whereas it is neglected in Klos et al. (2002).

Finally, we define the conditions for the equivalence of Eqs. (6.1a)- (6.1c) with our solution Eqs. (3.4). Eqs. (3.4) is applicable for any water residence time pdf $f(\tau)$, Gaussian or non-Gaussian. Only for the specific form of $f(\tau)$ consistent with the advection-dispersion equation, as defined in Eqs. (4.2), with a and c defined as

$$a = \frac{U^2}{4D_x} \quad ; \quad c = \frac{x}{\sqrt{D_x}} \tag{6.2}$$

is the system Eqs. (6.1a)- (6.1c) equivalent to the solution Eq. (3.5). Note that the definition of a, c in Eq. (4.3), and in Eq. (6.2) implies the classical relationships

$$\tau_m = \frac{x}{U} \qquad \sigma_\tau^2 = \frac{2\,D_x\,x}{U^3}$$

It is emphasized here that the dispersion coefficient D_x quantifies the variability in advection within fractures, and not the small-scale ("pore-scale") dispersion processes.

Since we have used Eq. (4.2), with a and c as defined in Eq. (4.3), our model is in fact equivalent to the transport model used in Klos et al. (2002) (neglecting the impact of immobilized colloids on sorption). Note that with the appropriate definition of the retention function (denoted as $\mathcal{F}$ in Eq. (C7)-(C8) in Cvetkovic (2000)) that is consistent with unlimited diffusion/sorption, the transport model Eq. (A.7), or Eq. (A.9), was already presented in Cvetkovic (2000).

6.2 Experimental considerations

For tracer experiments, it is of interest to identify the ranges of controlling parameters within which observation of CFRT are possible. It is plausible that we may be able to at least constrain sorption parameters in the laboratory by conducting batch experiments of the type presented in Lu et al. (1998, 2000). In that case, it is of interest to know what potential impact the constrained range of α_f may have on the outcome of CFRT tests.

The two key (uncertain) parameters in our investigation are the filtration rate ϵ and the forward sorption rate α_f. These two parameters have opposing effects on CFRT: Whereas increase of ϵ reduces the impact of colloids, increase of α_f enhances CFRT (especially if sorption onto colloids is almost irreversible).

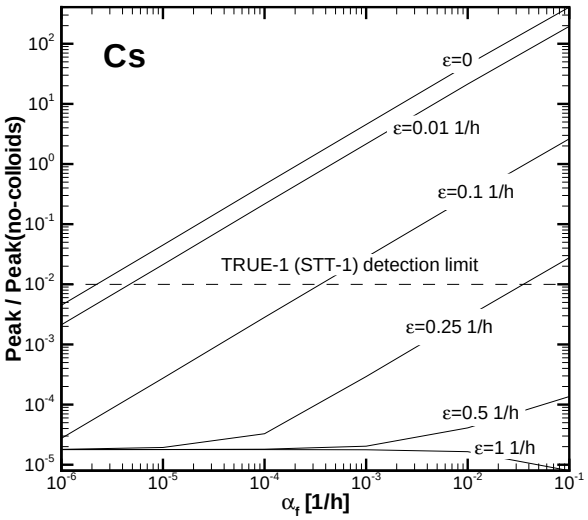

Figure 6.1: Dependence of peak normalized expected Cs discharge relative to the expected peak Cs discharge without colloids, on the sorption rate α_f and for different filtration rates ϵ. The detection limit applicable for TRUE-1 is also noted. The curves for X and Y are obtained by numerical Laplace inversion of Eqs. (3.5) with Eq. (4.4).

In order to identify the detectable parameter range for CFRT, we define a ratio between the early Cs discharge peak (computed with Eq. (3.5)), and the Cs discharge peak in the absence of colloids. The dependence of this ratio on α_f and for different filtration rates, is illustrated in Fig. 6.1. Clearly, the early peak is reduced with stronger filtration, and likewise, it is reduced for decreasing α_f. From the TRUE-1 BTCs for Cs, e.g., in STT-1 tests, it is seen that Cs was detected up to 1% of the Cs peak discharge; we assume this to be the detection limit, i.e., 0.01 of the peak (without colloids). The line of the detection limit is shown in Fig. 6.1.

With Fig. 6.1 established, we plot the intersection points between the detection limit (dashed) line, and the solid lines. The result is plotted in Fig. 6.2. The symbols in Fig. 6.2 effectively define the detectable and non-detectable regions of the parameter space α_f, ϵ. If we can estimate α_f in the laboratory, and place the point in Fig. 6.2, then we can identify the maximum value of ϵ for which detection of the early peak of Cs breakthrough is still possible. Not detecting the early peak of Cs in the CFRT tests could then imply that the field-scale ϵ is greater than the limiting value obtained from Fig. 6.2 (say ϵ^*); this implies that ϵ^* sets an important constraint and could be used as a lower bound of ϵ, for instance, when analyzing the potential impact of CFRT on the performance assessment scale.

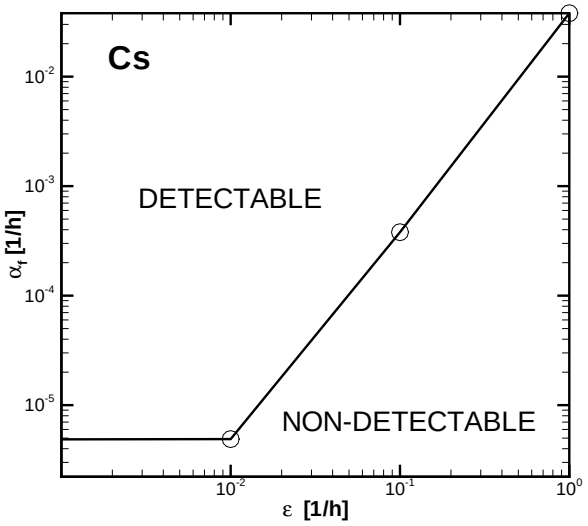

Figure 6.2: Detectable and non-detectable regions of the parameter space α_f, ϵ for Cs and $\tau_m = 100$ h. The symbols in the figure where obtained as intersection points between the solid lines and the horizontal dashed line in Fig. 6.1.

Chapter 7

Conclusions

Based on our sensitivity study of CFRT for two tracers under TRUE experimental conditions, we draw the following conclusions.

- Impact of colloids is more apparent (and presumably observable) for a strongly sorbing tracer such as Cs, and less apparent (and presumably not observable) for a moderately sorbing tracer such as Ba.
- Longer mean water residence time on the order of 100 h is preferable for CFRT to be observable in a tracer test, compared to a shorter water residence time on the order 10 h.
- Irreversible sorption yields the strongest impact of CFRT; however, even for relatively strong reversibility with $f_r = \alpha_r/\alpha_f = 0.1$, the impact of reversibility is modest; thus it appears that reversibility is not an important issue for experimental time scales.
- Diffusion limitations affect the tailing of the BTCs but not the initial peak; hence, it does not affect CFRT in a manner that is relevant for tracer test time scales, and for the sorbing tracers that are candidates for the tests, such as Cs.
- Finite injection has a relatively small impact on CFRT, where the early peak is somewhat reduced; thus the injection can be carried out in a similar manner as was done for the TRUE-1 tests.
- Filtration of colloids can have a significant effect on CFRT, as expected; it strongly reduces the impact of CFRT for $\epsilon > 0.01$ 1/h, but has a relatively modest impact for $\epsilon < 0.01$ 1/h.

- In TRUE-1 STT-1 test with Cs, 1% of the peak was the detection limit. If we assume a comparable detection limit ratio, i.e., 0.01 of the Cs peak without colloids, then we identified the region of the parameters space for ϵ, α_f which would be detectable in a CFRT test.

- For $\epsilon < 0.01$ 1/h, CFRT of Cs would be detectable for α_f as low as $5{\cdot}10^{-6}$ 1/h; for increasing filtration rate, increasingly higher sorption rate is required for CFRT to be detectable. For $\epsilon > 0.01$ 1/h, we established a linear log-log relationship which is simple to use once an estimate of either α_f and/or ϵ is available.

- The forward sorption rate α_f is an important controlling parameter which can, and should, be estimated in the laboratory say using batch tests of the type presented by Lu et al. (1998, 2000).

In the present analysis, we have not explicitly accounted for the tracer exchanges between the solution and immobile colloids as was done in Klos et al. (2002); such exchanges can be implicitly accounted for, for instance, in the surface sorption coefficient R_f. However, such exchanges can be incorporated explicitly in the solution of the type Eq. (3.4), as shown in Cvetkovic and Painter (2004). Furthermore, the detection limit assumed here was only approximate and it is likely that current detection technology and experimental conditions would allow for a detection, expressed as a fraction of the peak, that is lower than 1%. It is relatively easy to re-define the detectable/non-detectable regions of the parameter space α_f, ϵ in Fig. 6.2 by changing the assumed detection limit.

Appendix A

Governing equations

The general mass transport model which captures the key kinetic interactions (diffusion/sorption in the rock matrix and first-order kinetic sorption onto colloids), is written as:

$$R_f \frac{\partial C}{\partial t} + \frac{\partial C}{\partial \tau} = \frac{\theta D}{b} \frac{\partial C_m}{\partial z} \Big|_{z=0} - \alpha_f C + \alpha_r S - \lambda R_f C \tag{A.1a}$$

$$R_c \frac{\partial S}{\partial t} + \frac{\partial S}{\partial \tau} = \alpha_f C - \alpha_r S - \epsilon S - \lambda R_c S \tag{A.1b}$$

$$R_m \frac{\partial C_m}{\partial t} = D \frac{\partial^2 C_m}{\partial z^2} - \lambda R_m C_m \tag{A.1c}$$

The quantities given in Eqs. (A.1a)-(A.1c) are defined as:

$2b$ – "effective" aperture of fracture [L]

D – pore diffusivity of rock matrix [L^2/T]

θ – porosity of rock matrix [-]

ϵ – filtration rate [1/T]

C – mobile tracer concentration in fracture [M/L^3]

C_m – immobile tracer concentration in rock matrix [M/L^3]

R_m – retardation coefficient in rock matrix [-]

R_f – retardation coefficient for surface sorption [-]

R_c – retardation coefficient for colloids [-]

S – tracer concentration on colloids in fracture [M/L^3]

α_f – forward sorption rate from solution to colloids [1/T]

α_r – reverse sorption rate from solution to colloids [1/T]

λ – decay rate [1/T]

z – distance perpendicular to plane of fracture [L]

τ – water residence time [T]

t – time [T]

In the absence of colloids, $\alpha_f = \alpha_r = 0$, whereby Eq. (A.1a) and Eq. (A.1c) reduce to the well known system of equations for radionuclide transport in rock fractures. We emphasize that Eqs. (A.1a)- (A.1c) are written along trajectories (Lagrangian formulation), hence the one-dimensional formulation with the water residence time τ as the independent variable (Cvetkovic and Dagan, 1994). Also, note that advective transport takes place along trajectories embedded in a two-dimensional random velocity field of a single fracture (Cvetkovic et al., 1999; Cvetkovic, 2000)

We are interested to quantify transport in terms of radionuclide discharge; hence we multiply Eqs. (A.1a)- (A.1c) by the flow rate q which advects the radionuclide from the injection point (A) to the detection point (B), to obtain:

$$R_f \frac{\partial X}{\partial t} + \frac{\partial X}{\partial \tau} = \frac{\theta\, D}{b} \frac{\partial X_m}{\partial z} \mid_{z=0} \; -\alpha_f\, X + \alpha_r\, Y - \lambda\, R_f\, X \tag{A.2a}$$

$$R_c \frac{\partial Y}{\partial t} + \frac{\partial Y}{\partial \tau} = \alpha_f\, X - \alpha_r\, Y - \epsilon Y - \lambda\, R_c\, Y \tag{A.2b}$$

$$R_m \frac{\partial X_m}{\partial t} = D \frac{\partial^2 X_m}{\partial z^2} - \lambda\, R_m\, X_m \tag{A.2c}$$

where $X \equiv qC$, $Y \equiv qS$ and $X_m \equiv qC_m$; note that the quantity $X_m \equiv qC_m$ does not have a direct physical interpretation and can be considered in Eqs. (A.1a)-(A.1c) as an auxiliary quantity.

We first solve Eq. (A.2c) in the Laplace domain to obtain

$$\widehat{X}_m = C_1 \, \exp\left(-z\sqrt{s\, R_m/D}\right) + C_2 \, \exp\left(z\sqrt{s\, R_m/D}\right)$$

where C_1, C_2 are constants with respect to z, and s is replaced by $s + \lambda$ if decay is to be accounted for. For zero flux boundary condition $\partial X_m/\partial z = 0$ at $z = \zeta$, we obtain (Cvetkovic et al., 1999)

$$\frac{\partial X_m}{\partial z} \mid_{z=0} = -\widehat{X}\, A(s)\, \sqrt{s\, R_m/D} \tag{A.3}$$

where

$$A(s) \equiv \frac{\exp\left\{2\,\zeta\sqrt{s\, R_m/D}\right\} - 1}{\exp\left\{2\,\zeta\sqrt{s\, R_m/D}\right\} + 1} \tag{A.4}$$

Taking the Laplace transform of Eqs. (A.2a)-(A.2b), and inserting Eq. (A.3) into Eq. (A.2a), we get

$$\frac{d\widehat{X}}{d\tau} = a_{11}\, \widehat{X} + a_{12}\, \widehat{Y} \tag{A.5}$$

$$\frac{d\widehat{Y}}{d\tau} = a_{21}\,\widehat{X} + a_{22}\,\widehat{Y}$$

where the components of a_{ij} are defined by:

$$a_{11} \equiv -s\,R_f - k\,\kappa\,A(s)\sqrt{s} - \alpha_f$$

(A.6)

$$a_{12} \equiv \alpha_r \qquad a_{21} \equiv \alpha_f \qquad a_{22} \equiv -s\,R_c - \alpha_r - \epsilon$$

where $k = 1/b_{\mathrm{ret}}$ is the inverse effective half-aperture for the linearized expression $\beta = k\,\tau$, and $\kappa = \theta\,\sqrt{R_m D}$. Note that with $A(s)$ defined in Eq. (A.4), we account for a finite retention zone (limited diffusion). For $\zeta \to \infty$, $A(s) \to 1$ and Eq. (A.5) converge to the unlimited diffusion case.

The boundary condition for X and Y in Eq. (A.5) is $X(t,0) = X_0(t)$ and $Y(t,0) = 0$, i.e. $\widehat{X} = \widehat{X}_0$ and $\widehat{Y} = 0$, with an initially tracer-free porous medium. The solution of Eq. (A.6) is written as

$$\widehat{X} = A_1\,\exp\left(\Lambda_1\,\tau\right) + A_2\,\exp\left(\Lambda_2\,\tau\right)$$

(A.7)

$$\widehat{Y} = B_1\,\exp\left(\Lambda_1\,\tau\right) + B_2\,\exp\left(\Lambda_2\,\tau\right)$$

where

$$A_1 = \frac{\Lambda_1 - a_{11}}{\Lambda_1 - \Lambda_2} \qquad A_2 = \frac{a_{11} - \Lambda_2}{\Lambda_1 - \Lambda_2}$$

$$B_1 = A_1\,\frac{a_{21}}{\Lambda_1 - \Lambda_2} \qquad B_2 = -B_1 \tag{A.8}$$

$$\Lambda_{1,2} = \frac{1}{2}\,\left(a_{11} + a_{22}\right) \pm \frac{1}{2}\,\left[\left(a_{11} - a_{22}\right)^2 + 4\,a_{12}\,a_{21}\right]^{1/2}$$

satisfying the pulse condition $X(t,0) = \delta(t)$, $\widehat{X} = 1$ and $Y(t,0) = 0$.

In case the reversibility is sufficiently low such that sorption is approximated as irreversible with $\alpha_r \to 0$, we have

$$\widehat{X} = \mathrm{e}^{-\tau\,(s\,R_f + \kappa\,k\,\sqrt{s} + \alpha_f)}$$

(A.9)

$$\widehat{Y} = \frac{\alpha_f}{W} \, \mathrm{e}^{-\tau(s\,R_c+\epsilon)} \, \left(1 - \mathrm{e}^{-W\,\tau}\right)$$

where

$$W(s) \equiv s\,R_f + \kappa\,k\,\sqrt{s} + \alpha_f - s\,R_c - \epsilon \tag{A.10}$$

Real solutions for X and Y can be obtained by numerical inversion of $\widehat{X}$ and $\widehat{Y}$, or alternatively, can be characterized by their moments.

Bibliography

Byegård, J., Johansson, H., Skålberg, M., and Tullborg, E.-L. (1998). The interaction of sorbing and non-sorbing tracers with different Äspö rock types: Sorption and diffusion experiments in the laboratory scale. SKB Technical Report TR-98-18, Swedish Nuclear Fuel and Waste Management Co.

Cvetkovic, V. (2000). Colloid-facilitated tracer transport by steady random ground-water flow. *Physics of Fluids*, 12:2279–2294.

Cvetkovic, V. (2003). Potential impact of colloids on the plutonium migration at the Äspö site. SKB Report R-03-16, Swedish Nuclear Fuel and Waste Management Co.

Cvetkovic, V., Cheng, H., and Selroos, J. (2000). Evaluation of tracer retention understanding experiments (first stage) at Äspö. SKB International Cooperation Report ICR-00-01, Swedish Nuclear Fuel and Waste Management Co.

Cvetkovic, V. and Dagan, G. (1994). Transport of kinetically sorbing solute by steady random velocity in heterogeneous porous formations. *Journal of Fluid Mechanics*, 265:189–215.

Cvetkovic, V. and Painter, S. (2004). Colloid-facilitated tracer transport with multiple sorption sites in heterogeneous porous media. in preparation.

Cvetkovic, V., Selroos, J. O., and Cheng, H. (1999). Transport of reactive tracers in rock fractures. *Journal of Fluid Mechanics*, 378:335–356.

Klos, R., White, M., Wickham, S., Bennett, D., and Hicks, T. (2002). Quantitative assessment of the potential significance of colloids to the KBS-3 disposal concept. Technical Report SKI 02:34, Swedish Nuclear Inspectorate.

Lu, N., Conca, J., Parker, G., Leonard, P., Moore, B., Strietelmeier, B., and Triay, I. (2000). Adsorption of actinides onto colloids as a function of time, temperature,

ionic strength, and colloid concentration. Technical Report LA-UR-00-5121, Los Alamos National Laboratory.

Lu, N., Triay, I., Cotter, C., H.D.Kitten, and Bentley, J. (1998). Reversibility of sorption of Plutonium-239 onto colloids of Hematite, Goethite, Smectite and Silica: A milestone final report of YMP. Technical Report LA-UR-98-3057, Los Alamos National Laboratory.

Neretnieks, I. (1980). Diffusion in the rock matrix: An important factor in radionuclide retention. *Journal of Geophysical Research*, 85(B8):4379–4397.

Poteri, A., Billaux, D., Dershowitz, W., Gomez-Hernandez, J., Cvetkovic, V., Hautojärvi, A., Holton, D., Medina, A., and Winberg, A. (2002). Final report on the TRUE Block Scale project 3. Modelling of flow and transport. SKB Technical Report TR-02-15, Swedish Nuclear Fuel and Waste Management Co.

Winberg, A., Andersson, P., Hermanson, J., Byegård, J., Cvetkovic, V., and Birgersson, L. (2000). Final report on the first stage of the tracer retention understanding experiments. SKB Technical Report TR-00-07, Swedish Nuclear Fuel and Waste Management Co.